UCRL- 1836

UNCLASSIFIED

UNIVERSITY OF CALIFORNIA — BERKELEY

TWO-WEEK LOAN COPY

This is a Library Circulating Copy which may be borrowed for two weeks. For a personal retention copy, call Tech. Info. Division, Ext. 5545

RADIATION LABORATORY

DISCLAIMER

This document was prepared as an account of work sponsored by the United States Government. While this document is believed to contain correct information, neither the United States Government nor any agency thereof, nor the Regents of the University of California, nor any of their employees, makes any warranty, express or implied, or assumes any legal responsibility for the accuracy, completeness, or usefulness of any information, apparatus, product, or process disclosed, or represents that its use would not infringe privately owned rights. Reference herein to any specific commercial product, process, or service by its trade name, trademark, manufacturer, or otherwise, does not necessarily constitute or imply its endorsement, recommendation, or favoring by the United States Government or any agency thereof, or the Regents of the University of California. The views and opinions of authors expressed herein do not necessarily state or reflect those of the United States Government or any agency thereof or the Regents of the University of California.

UCRL-1836

Unclass Physics Dist.

UNIVERSITY OF CALIFORNIA

Radiation Laboratory

Contract No. W-7405-eng-48

ATOMIC NUMBER DEPENDENCE OF NEUTRAL MESON YIELD FROM PROTON BOMBARDMENT

Richard Wayne Hales

(Thesis)

June, 1952

Berkeley, California

TABLE OF CONTENTS

		page
I.	ABSTRACT	3
II.	INTRODUCTION	4
	A. Artificial Production of Mesons	4
	B. Interactions of Mesons with Matter	4
	C. A-Dependence of Meson Production	5
	D. Neutral Meson Yield Versus A from Protons	6
III.	PROCEDURE	9
IV.	DETAILS OF THE EXPERIMENT	11
	A. Targets	11
	B. Counters	18
	C. Electronics	20
V.	CORRECTIONS	23
VI.	RESULTS	29
VII.	CONCLUSIONS	32
VIII.	PROPOSED EXTENSION OF π^0 YIELD VERSUS "A" EXPERIMENT	39
IX.	ACKNOWLEDGMENTS	40
X.	APPENDIX	41
XI.	REFERENCES	42
XII.	ILLUSTRATIONS	45

I. ABSTRACT

The relative yield of neutral mesons from various elements in the reaction (p, π^0) has been determined. Single photons from neutral meson decay were observed at 135° to the proton beam in the laboratory system. Detection was by means of a pair scattering detector composed of a converter and two anthracene crystal telescopes in juxtaposition.

The yield in the range of elements from hydrogen to sodium is essentially proportional to the number of neutrons; in the elements aluminum to lead it is proportional to $(N/A)\ A^{2/3}$. These results are compatible with a mean free path in nuclear matter for the neutral mesons of approximately 10 a_o where a_o is given by the ratio $R/A^{1/3}$, R being the radius of the nucleus.

II. INTRODUCTION

A. Artificial Production of Mesons

Since the last war a great deal has been done in experimental meson physics to determine the fundamental properties of mesons and the nature of their interaction with other matter. Artificially produced mesons were first reported in 1948 by Gardner and Lattes[1] when they detected negative pions from the Berkeley synchrocyclotron. Under controlled laboratory conditions certain information has been obtainable with greater accuracy than was possible in cosmic ray work.

Neutral mesons were first observed by Bjorklund, Crandall, Moyer, and York[2] when targets were bombarded by 340 Mev protons. Steinberger, Panofsky, and Steller[3] observed coincidences between decay gamma rays from photo-produced neutral mesons, verifying the decay scheme

$$\pi^0 \longrightarrow 2\gamma$$

postulated by Tanikawa[4]. Many experimenters have contributed to the knowledge of the physical properties of pions; such as charge, spin, intrinsic parity and lifetime. Of additional interest is the interaction of these mesons with matter.

B. Interactions of Mesons with Matter

Mesons were originally postulated by Yukawa[5] to explain the forces between nucleons. The interaction of mesons with matter in meson production, scattering from nuclei, and absorption will yield information on meson-nucleon forces which any field theory must be tailored to fit.

In general the pion-nucleon interaction is a strong one, of the type necessary to account for nucleon-nucleon forces in terms of particle exchange. Single pions are produced in the laboratory with presently available energies in either nucleon or photon initiated events. Multiple pion production occurs in cosmic ray events where the necessary energies are available. In comparison with this the muon-nucleon interaction is weak; there seems to be no evidence for muon production during events of the type mentioned above. The capture of negative pions at rest to form stars is another indication of strong interaction. Negative muons, on the other hand, decay when stopped in material of low atomic number, Z, and even though the probability of capture increases with Z (the probability for decay and capture are equal at $Z \approx 10$)[6] there is no evidence for production of stars of ionizing particles. Instead the nucleus seems to be left with little excitation, capable only of neutron and gamma ray emission. Thus the production and mode of disappearing while at rest indicate that the pion is of primary interest as far as nucleon-nucleon forces are concerned, and that the muon is not directly related to nuclear forces.

In keeping with this strong interaction, information on the scattering of charged pions[7] by protons indicates that this reaction is very energy dependent and is compatible with a fourth power dependence on the pion momentum. The absorption and inelastic scattering of pions by other nuclei also indicate a strong energy dependence[8][9][10], with cross sections being geometric at energies of 85 Mev and above[11][12].

C. A-Dependence of Meson Production

It is entirely possible for the meson to scatter or be absorbed in the same nucleus in which it is produced. Mozley[13] and McMillan

pointed out the implications of this possibility in connection with meson production from complex nuclei. In a recent article, R. Wilson[31] has indicated that for high energy mesons (>70 Mev) there is a near 90 per cent probability of being reabsorbed by the parent, and a neighboring, nucleon. Under these conditions only those nucleons on the surface would essentially contribute to the meson yield. Studies of charged photomeson production from various nuclei ranging from hydrogen to lead, at meson energies of 42, 50, and 76 Mev[13][14] show yields which are generally proportional to the nuclear surface. Since nuclear matter is incompressible, the volume of the nucleus is proportional to A, the number of nucleons in the nucleus. Thus the surface is proportional to $A^{2/3}$. The neutral photomeson yield, versus A, also shows an $A^{2/3}$ dependence in elements from lithium to lead[15]. The relative yields of charged pions from protons on various nuclei at 0°[16] and 135°[17] to the beam is not yet done with good statistics. Indications to date are that the yield is not proportional to the number of nucleons and that there is strong absorption in the high Z nuclei.

D. Neutral Meson Yield versus A from Protons

Neutral pions produced from protons are presumed to be the same as those produced by photons and by proton capture of negative pions. Due to experimental difficulties coincident decay gamma rays have not been observed from proton produced π^{o}'s; however, the photon energy spectrum from these π^{o}'s shows quite definitely that they are the same as those produced by the other reactions. It was of interest to see how the yield of π^{o}'s from various targets compared with other work done as given above. Specifically, the question arose as to how absorption effects in the nucleus,

if any, manifest themselves in terms of cross sections.

Work already done on the light nuclei[18] indicated a yield from only the neutrons in the nucleus. The reason for this can be seen by considering the reaction

$$p + p \rightarrow p + p + \pi^0$$

where the π^0 is assumed to be a pseudoscalar meson. Evidence to date indicates that mesons from nucleon-nucleon collisions are created into P states. The available energies are such that the resulting nucleons should be left in S states. There is no initial state for the two protons, in this case, which will allow this final combination of meson and proton angular momenta. It is possible for the meson to come off in an S state, but this requires either the incoming protons or the resulting protons to be in a triplet P state. Whitehead and Richman[32] set an upper limit of 9 per cent for the ratio of meson yield in the S state to P state in the reaction

$$p + p \rightarrow \pi^+ + d$$

If this same ratio is applicable to the π^0 production reactions, one would assume the π^0 yield from protons in the nucleus to be down by a factor of approximately ten compared with the yield from neutrons where production of the mesons in the P state <u>is</u> allowed. Such a favoring of production from neutrons was seen to hold true in the nuclei Be^9, B^{10}, B^{11}, and C^{12}. The yield from hydrogen is further reduced because it is a free nucleon and has no internal nuclear momentum to add to the momentum of the bombarding proton to raise the available energy.

It was hoped that further work might show whether or not this effect continues in the heavier elements. Because the production process is so energy dependent, there were indications that the effect of the internal momenta of the nucleons - especially in the lightest nuclei - might manifest itself in the comparison of cross sections. It was also thought that perhaps nuclear shell structure might have some noticeable effect.

III. PROCEDURE

Targets were bombarded in the external proton beam of the 184" synchrocyclotron by protons of approximately 340 Mev. This external beam is obtained by scattering the protons of the circulating beam into a magnetic channel which deflects them through the fringing magnetic field into an evacuated pipe. The beam is collimated; its direction changed by an auxiliary steering magnet, which causes it to pass (inside the pipe) through the fifteen feet of concrete shielding surrounding the cyclotron into the experimental area called the "cave". (See Fig. 1.) The end of the evacuated pipe (the "snout") just protrudes into the cave from the concrete shielding. The last 40 inches of the pipe preceding the snout is filled with brass capable of adjustable collimation from $\frac{1}{4}$ to 2 inch diameter.

An ionization chamber was placed immediately behind the snout to record the proton beam current.

A lead wall fourteen inches thick with a 3 inch diameter hole was erected to help attenuate neutrons and other particles coming from reactions in the cyclotron itself and in the collimating system. Targets were placed at approximately eight inches following this lead wall.

At an angle of 135° to the beam direction two sets of photon counters viewed the target. Each counter consisted of four anthracene crystal - 1P21 photomultiplier tube units. (See Fig. 2.) The outputs of the phototubes were mixed in fast double coincidence in the cave; the two coincidence pulses from each counter were mixed in slow double coincidence in the counting area after amplification and pulse shaping. This

meant that time coincident pulses from each of the four units in a counter were required to register an event; namely, the detection of a single photon. The use of two counters had a dual purpose. In addition to speeding up the collection of data, it permitted mixing of the outputs of the two counters to check on the possibility of coincidences between gamma rays. A calculation assuming isotropic meson distribution shows that less than one coincidence count in 70 hours is to be expected. That there were no indicated real $\gamma - \gamma$ coincidences in all the runs of this experiment, therefore is not surprising.

A corroboratory run was performed using the pair spectrometer arrangement of Crandall and Moyer. The arrangement of the components is shown in Fig. 3. A target was bombarded at the rear of the cave. Photons emitted at 90° passed through a collimated hole in the cave wall, through a second collimation placed in a magnetic field, and then to the pair spectrometer magnet. A 41.4 mil tantalum radiator was used to convert the photons into electron pairs. Detection of the electrons was in double chamber proportional tubes filled with CO_2 and Argon.

The pair spectrometer was placed at the intersection of the high energy neutron beam line (this line is tangent to the 81 inch radius) and the 90° angle to the cave target. By having the pair spectrometer look at an internal target at the 81 inch radius, proportional counter plateaus could be determined with high counting rates. The pair spectrometer was then turned to look at the cave target.

IV. DETAILS OF THE EXPERIMENT

A. Targets

In designing targets for this experiment it was necessary to consider the loss of energy of the incoming protons in passing through the target matter, conversion of the neutral meson decay gamma rays into electron pairs in the target, production of background particles, and the limitation imposed by available sizes and shapes of some elements in their pure form. The targets were not specifically designed to keep a single factor constant. Instead the targets in a given comparison group were made with approximately the same gm/cm^2 thickness. This meant that in the same region of the periodic table the energy degradation would be nearly the same and the background events would be similar. The thickest targets were five gms/cm^2 thick. This corresponds to a maximum energy degradation (for lithium) of 14 Mev. Thicknesses of this order of magnitude and less, combined with small lateral extent, kept corrections for pair conversion in the target to ten per cent or less except for carbon tetrachloride and calcium. A discussion of pair production corrections is given in another section.

The diversity of physical states and geometrical shapes available necessitated the use of the following six series of targets. Various elements from hydrogen to lead were bombarded. Yields were compared to carbon as a reference.

Series 1. H_2O, D_2O, C, O_2. This series was run by Hildebrand and Knable[18]. The use of liquid oxygen necessitated use of a dewar vessel. This was constructed of aluminum with a four mil inner wall,

14 mil outer wall, and two inch diameter liquid chamber. The liquids were all bombarded in this container; the carbon was machined in the shape of a cylinder of comparable size and shape.

Series 2. H_2O, D_2O, C (Graphite), CH_2 (polyethylene), and CCl_4. These materials were contained in brass cylinders $3\frac{1}{2}$ inches outside diameter, $3\frac{1}{4}$ inches inside diameter. Aluminum foil of 0.003 inch thickness was cemented over the faces of the cylinder with araldite. Because of the different thermal coefficients of expansion of the brass cylinder and aluminum foils, the foils were stretched taut during the process of baking the araldite and the subsequent cooling.

The target thicknesses were such that corrections for pair production were necessary in some cases (See section on corrections). This is shown in Table I, where t = target thickness, λ = mean free path for pair production by 100 Mev photons, and $\theta = 45^\circ$ = acute angle of observation with respect to target surface normal.

TABLE I

Target	t	λ = m.f.p.	t/λ	$\frac{1}{2}\frac{t}{\lambda\cos\theta}$	$\frac{t}{\lambda\cos\theta}\frac{1}{1-e^{-t/\lambda\cos\theta}}$
H_2O	0.750 in.	31.5 in.	0.024	0.017	1.017
H_2O	1.500	31.5	0.048	0.034	1.034
D_2O	0.750	31.5	0.024	0.017	1.017
D_2O	1.500	31.5	0.048	0.034	1.034
C	0.500	23	0.022	0.0155	0.016
C	1.000	23	0.044	0.031	1.031
CH_2	1.000	46.7	0.021	0.015	1.015
CH_2	1.500	46.7	0.032	0.0226	1.023
CCl_4	0.750	8.42	0.089	0.063	1.064
CCl_4	1.500	8.42	0.178	0.126	1.131

The H yield was obtained by CH_2, C subtraction; the D yield by D_2O, H_2O subtraction (where the H_2 yield was neglected); the Cl by CCl_4, C subtraction; and the O yield was taken to be equal to that of H_2O because of the small hydrogen cross section.

Series 3. C, Ca. Calcium was available in elemental form large enough to permit a target 0.928 inch diameter x 3/16 inch and of mass 20.44 gms to be machined. A graphite target of similar dimensions and mass 21.42 gms was also made. When not in use the calcium target was kept immersed in a light mineral oil to retard the rate of oxidation.

The pair production correction factors were 1.034 and 1.118 for carbon and calcium respectively. These corrections are the cylinder corrections (See section on corrections).

Series 4. Li, Be, B^{10}, B(natural), C, Na, K. The lithium target was machined under a light mineral oil and stored in the oil to prevent oxidation. The beryllium target was prepared by the Radiation Laboratory machine shop in a specially ventilated room. The two boron isotopes were each available as one inch diameter x $\frac{1}{4}$ inch compressed powder cylinders of less than one per cent oxygen impurity. There were four discs of each isotope making a one inch thickness for the targets. Carbon was obtained in one inch diameter stock.

Sodium and potassium could not be machined because of their softness and great chemical activity. By making use of the low melting points which these metals have, it was possible to cast them. Sodium has a density of 0.97 gm/cm^3. Potassium has a solid density of 0.86 gm/cm^3 and a liquid density of 0.83 gm/cm^3. It is necessary, therefore, to have an oil of density less than 0.83 gm/cm^3. The melting points of

the two elements are 97.5°C and 62.3°C respectively. The metal to be cast was placed in a beaker of suitable size and covered with mineral oil. A gas flame was used to heat the contents of the beaker above the metallic melting point. Upon melting, the metal and oxide stratified into metal and slag. The contents of the beaker were poured into a glass centrifuge tube of one inch inside diameter and approximately 1/32 inch thickness. After the metal had solidified the excess oil was poured off, the glass tube broken and removed, the solid metal target cut to the desired length and reimmersed in oil.

When in use these targets were suspended on a 0.001 inch aluminum foil (to protect the rest of the support from the chemical activity). The alkaline metal targets were bombarded in the open air for periods up to thirty minutes at a time. Before each use of these targets the oxide was scraped from the ends with a scalpel and the oil wiped from them. During the time the sodium and potassium were exposed to air, the oxide coating at no time became more than a few mils thick or the mass increase more than a fraction of one per cent. Because the beam was collimated to a smaller diameter than the targets, only the oxidation on the ends needed to be considered. This was negligible.

For all but lithium, sodium, and potassium, the cylindrical pair production correction was used. For the three named, the cylindrical correction was taken with the radius increased by the factor $1/\cos\theta$ where $\theta = 45^\circ$ is the angle between the target axis and direction of the counter. The corrections are given in Table II, where t = thickness, R = radius, λ = mean free path.

TABLE II

Elem	t	R	λ	R/λ	Correction Factor $\frac{1}{1-(16/3\pi)\,R/\lambda}$
Li	3.505 in.	0.501 in.	156 in.	0.0032	1.006
Be	0.750	0.500	33.8	0.0148	1.026
B^{10}	1.023	0.500	24.2	0.0206	1.036
B(nat)	0.916	0.500	25.8	0.0194	1.032
C	0.896	0.509	23	0.0221	1.038
Na	1.483	0.515	22.2	0.0232	1.058
K	1.630	0.505	13.9	0.0363	1.096

Series 5. C, Al, Cu, Pb. These four of the "usual" elements were designed with pair conversion in the target being the major consideration. The mean free paths for pair conversion of 100 Mev photons in these elements are 22, 6.7, 1.02, and 0.342 inches respectively (as calculated from curves given by Heitler[19] and checked within 25 per cent by measuring the photon attenuation in these materials by a pair spectrometer). It was experimentally determined that the photon yield from lead was roughly proportional to the target thickness for thicknesses up to 1/4 λ. The lead target was chosen to be 1/10 λ thick to be well within the region of calculable correction. The other targets were then chosen to have approximately the same number of gms/cm^2.

The data of targets used is contained in Table III.

TABLE III

Elem	t	t	λ=m.f.p.	t/λ	Correction Factor $\frac{t}{\lambda \cos\theta} \frac{1}{1-e^{-t/\lambda\cos\theta}}$
C	1.02 gm/cm^2	0.250 in.	22	0.011	1.008
Al	0.86	0.125	6.7	0.019	1.013
Cu	0.73	0.032	1.02	0.031	1.022
Pb	0.98	0.034	0.342	0.099	1.072

Series 6. D_2, He, N_2, A. These gases were bombarded in a stainless steel pressure chamber designed by R. Stephen White[20]. (Figures 4 and 5.) The target structure consisted of three concentric chambers, the inner for target gas, middle for coolant, and outer for an insulating vacuum. The gases deuterium and helium were compared. Liquid nitrogen was used as a coolant in the target and in a vapor trap in the high pressure pumping system. The stainless steel strength of the target at 77°K allowed pressures of 2200 psi to be maintained. A second comparison between nitrogen and argon was attempted, using ice water as the target and trap coolant. The gas characteristics and decline in steel strength with use at 0°C permitted only 1000 psi and 900 psi pressures, respectively, to be maintained in the heavier gases. The densities of the four gases used, along with hydrogen (which was not bombarded), under the conditions met, are given in Table IV. These densities were calculated from pressure volume relationships referred to in Table IV.

TABLE IV

Gas	Pressure	Temperature	Coolant	Density
H_2	2200 psi	77.6°K	Liquid N_2	0.0420[21] gm/cm^3
D_2	2200	77.6	"	0.0883[21]
He	2200	77.6	"	0.0745[22]
N_2	1000	10°C	Ice Water	0.0832[23]
A	900	10°C	"	0.110[24]

Series 7. C, Al, Pb. This series of targets was viewed by the pair spectrometer rather than the crystals. Because of the small solid angle subtended by the tantalum converter in the pair spectrometer, as seen from the target, and because of the large proton beam size ($3\frac{1}{2}$ inches diameter), it was necessary to have relatively large targets in order to obtain a reasonable counting rate. These targets were large both in terms of energy degradation of the proton beam and pair production in the target by the neutral meson gamma rays. The targets were designed to have the same total energy loss for protons. In a comparison, then, of relative cross sections the different targets would each see the same proton energy spectrum. This eliminated the need for a correction due to the dependence of the meson production cross section on proton energy. A large correction was required for the pair conversion. See section on corrections. These corrections are given in Table V.

TABLE V

Elem	Thickness Along Beam	ΔE	Pair Conversion Correction
C	3 inches 11.9 gm/cm^2	36.6 Mev	1.170
Al	2.04 " 14.5 gm/cm^2	36.6	1.620
Pb	0.383 " 11.1 gm/cm^2	18.3	1.560
	0.766 " 22.1 gm/cm^2	36.6	2.26

B. Counters

The counter scheme used has been reported previously[25], but for completeness will be briefly described.

Each photon detector consists of four anthracene crystals, each viewed by a 1P21 photomultiplier tube (Fig. 6). These were arranged in two adjacent telescopes with the crystals side by side. The crystals were 3/8 inch in thickness, the front crystals being one inch by two inches in area, the rear ones 1-3/4 x 2½ inches. These crystal sizes were chosen to reduce background without decreasing photon detection efficiency. The effective part of the converter was approximately 1½ inches. The coincidence counts from this strip were limited in solid angle by the size of the rear crystals. By choosing the front crystals to subtend approximately the same solid angle as the rear ones it was possible to cut down their volume and consequently the number of counts due to stray particles coming from the target.

The thickness of these crystals is such that an electron of three Mev will just get through the first crystal. Assuming the pair is produced in the rear layer of the converter, is not scattered in the first crystal,

and counts upon just reaching the second; it would require a six Mev photon to produce a coincidence in the telescope. Making allowances for these assumptions a more realistic threshold would be 15 - 20 Mev. This is out of the region of nuclear excitation and all photons seen should then be from π^0's. The validity of this argument is borne out by the agreement with the pair spectrometer run in which the lowest energy photon accepted was 65 Mev.

They were covered on five sides with 0.001 inch aluminum foil for high reflectivity. The covered crystal was then taped in a light-tight manner to a $1\frac{1}{2}$ inch diameter soft iron cylinder of 1/16 inch wall thickness. This iron cylinder fit snugly over the 1P21 phototube unit and provided magnetic shielding from the approximately 18 gauss stray field from the cyclotron encountered in the cave. Each photomultiplier glass envelope was tightly wrapped with 0.003 inch copper foil which was tied electrically to the photo-cathode. This seems to help reduce tube noise. This foil was covered by electrical tape to provide insulation against the approximately 1500 volts which it carried. The tube was then inserted in the magnetic shield-crystal combination, clamped in place with a set screw and the unit made light tight. When in use the iron shield was grounded as a precaution against failure of the insulation on the copper foil inside.

Lead and carbon sheets of $\frac{1}{4}$ and $1\frac{1}{4}$ inches respective thickness were placed one at a time between the target and counters, with the target face being two inches from the front crystals. These sheets, or converters, served two purposes: Firstly, they caused the high energy photons to form electron pairs which were then typically separated by scattering; and

secondly, they attenuated the flux of charged particles coming from the target. The thicknesses were chosen for equal stopping power for charged particles. The number of pairs from lead as compared to carbon for these thicknesses should be ten to one. Thus, by subtracting the number of counts with a carbon converter from the number with lead converter, the background is essentially subtracted out and one has a measure of pairs produced and, consequently, an indication of the relative number of photons coming from the target. The transition curve for lead showed a peak at approximately $\frac{1}{4}$ inch which is to be expected of photons of the order of 100 Mev whereas that for carbon showed a drop from zero converter thickness to $1\frac{1}{4}$ inches, then a gradual rise, which is compatible with the stoppage of charged particles and small pair cross section in carbon.

C. Electronics

Pulses from the 1P21 phototube were clipped and shaped in a tube base unit of electronic design due principally to R. Madey. Clipping to 5×10^{-9} second was done in $1\frac{1}{2}$ inches of RG 65/U delay line cable. The pulses were limited in pulse height by cutting off a 6AH6 pentode.

Coincidences were made, as shown inFig. 2, in crystal diode bridge coincidence units with time resolution of 5×10^{-9} second. The schematic drawing for this circuit is shown in Fig. 7. By careful balancing of circuit elements it was consistently possible to obtain coincident (two inputs) to feed-through (single input) pulse height ratios of 16 to 1.

The 5×10^{-9} second coincidence pulses were amplified to approximately 0.2 volt in a two stage linear amplifier in the same chassis with the coincidence tube. These pulses were then cabled to the counting room

of the cyclotron where they were further amplified and shaped. The second amplification was 300-400 times, giving coincidence pulses up to 80 volts. The feedthrough pulse heights were five volts or less. The linear amplifier outputs triggered gate circuits in which nearly square wave pulses of 0.5×10^{-6} second were formed. Two such pulses from a given counter were joined in a Rossi type coincidence circuit of 10^{-6} second resolution.

In order to cut down the accidental counts due to the individual crystal counting rates, the scaling circuits were gated on with each cyclotron pulse. The scattered-deflected cyclotron beam emerges from the vacuum chamber of the cyclotron into the air of the cave in pulses approximately 25 microseconds long, 60 times per second. The same radio-frequency pulse which is used to pulse the cyclotron injector was made to trigger a gating circuit which generated a 100 microsecond square wave gate. This could then be made to straddle the cyclotron beam in time and turned the scalers on only during this time.

The pulses sent to the counting room by the bridge coincidence units were a mixture of coincidences from electron pairs formed by a single photon and accidental coincidences formed by all counts in the phototube. These counts are caused not only by the charged particles going through the crystals (electrons, mesons, and protons), but also by the noise inherent in the tube. Pulses from the electrons find competition in the high pulse height region from other charged particles and in the low region from the tube noise. The electrons are of minimum ionization energy so their pulse heights do not extend as high as those of protons and mesons. As a consequence, there was no set of operating conditions under which all counts that would give rise to accidentals could be

discriminated against. Instead the beam intensity had to be set at such a level that the counting rate per unit time of extraneous counts was low enough that accidentals were a small fraction of the coincidence counts from electron pairs. Thus, there was no plateau region of operation and actual operating conditions were somewhat arbitrary; trustworthiness of results depended upon satisfactory stability of the conditions.

Operational conditions were picked by setting the photomultiplier voltage at 1.4 to 1.5 kilovolts and the linear amplifier gains at such a level (amplification of 300 - 400 times) that five volt maximum output pulses were given by the linear amplifier for feedthrough pulses (single input to the bridge coincidence). The discrimination levels of the variable gates were then set at 10 volts, or double this value.

With this operational set-up it became necessary to choose a beam intensity such that the accidental coincidences were a small fraction of those sought. The accidental coincidence counting rate per unit charge in the proton beam is linear with the beam intensity (or of higher order if the accidental coincidence is between more than two particles), whereas the electron pair counts are constant per unit beam charge. Thus by lowering the beam intensity to a suitable value the ratio of accidentals to non-accidentals could be reduced to an arbitrarily small value. In these experiments beam currents of $0.8 - 3.2 \times 10^{-11}$ ampere were used, depending on the target thickness.

V. CORRECTIONS

As stated in previous sections the main correction to be applied was for the decrease in number of photons reaching the counters owing to production of pairs in the target matter. An upper limit to the mean life for decay of the π^0 has been set at 5×10^{-14} second[26]. This means that one can consider all the decays as taking place in the target matter and hence the photons emanating from the target.

The correction to be applied was determined by finding the ratio of the number of photons produced to the number leaving the target. Certain simplifying assumptions were made. It was assumed that neutral mesons (and consequently photons) were produced in equal numbers throughout the target volume irradiated by the proton beam. This volume was determined either by the target geometry or an X-ray film exposed immediately behind the target. Actually the spacial density of protons in the collimated beam area is not constant but is a good approximation in this case where target dimensions are small compared to photon mean free paths. Included in this basic assumption is a second one; namely, that the energy of the proton beam is not degraded to the point of cutting down the number of mesons produced in the rear section of the target. Most of the targets were thin, with less than four Mev energy loss. This small change in energy would correspond to only a few per cent drop-off in production. Because the targets in a given comparison group had the same geometry, were approximately the same thickness in terms of energy loss, and because the fractional drop in production was small (in most cases) this was considered a legitimate assumption.

Two general geometries were considered and in addition the specific cases which applied to the targets used in the pair spectrometer run. The two general cases were for a flat slab with its surface perpendicular to the beam and a cylinder with axis perpendicular to the beam.

Slab. Consider the photons produced in a target sheet of thickness, t, in the elemental thickness dx and which are observed at an angle θ to the normal of the target (See Fig. 8).

Let n = number of photons produced per unit thickness.

λ = mean free path for pair production.

Then the number of photons produced in dx is n dx and the number produced in dx and leaving the target is $n\,dx\,e^{-\frac{x}{\lambda\cos\theta}}$

The total number leaving the target is

$$N = n\int_0^t e^{-\frac{x}{\lambda\cos\theta}}\,dx$$

$$= n\lambda\cos\theta\left[1 - e^{-t/\lambda\cos\theta}\right]$$

The total number produced is

$$N_0 = nt$$

Therefore, the correction factor is given as the ratio of those produced to those actually leaving the target or

$$N_0/N = \frac{t}{\lambda\cos\theta}\,\frac{1}{1 - e^{-t/\lambda\cos\theta}}$$

For $(t/\lambda)(\cos\theta) \simeq 0.05$ this simplifies to

$$N_0/N \simeq 1 + \frac{1}{2}\,t/\lambda\cos\theta$$

Cylinder. Again, consider the photons produced in the element $dx\, d\rho$ of a circular section of radius R (Fig. 8).

Let n = number of photons produced per unit area in the circle.

λ = mean free path for pair production

The number of photons leaving the target from $dx\, d\rho$ is

$$n e^{-x/\lambda} dx\, d\rho$$

and the number from the whole target is

$$N = \int_{-R}^{R} \int_{0}^{2\sqrt{R^2-\rho^2}} n e^{-x/\lambda} dx\, d\rho$$

Integrating over x and using the symmetry in ρ one gets

$$N = 2n\lambda \int_0^R \left[1 - e^{-\frac{2\sqrt{R^2-\rho^2}}{\lambda}}\right] d\rho$$

The integral may be simplified somewhat by making the substitution

$$\rho = R \sin\theta$$

$$d\rho = R \cos\theta \; d\theta$$

$$\sqrt{R^2-\rho^2} = R \cos\theta$$

The integral then becomes

$$N = 2n\lambda R \int_0^{\pi/2} \left[1 - e^{-\frac{2R\cos\theta}{\lambda}}\right] \cos\theta\, d\theta$$

Upon expanding the exponential in series form

$$N = 4nR^2 \int_0^{\pi/2} \left[\cos\theta - \frac{2R}{\lambda}\cos^2\theta + \frac{2}{3}\left(\frac{R}{\lambda}\right)^2 \cos^3\theta + \cdots\right] \cos\theta\, d\theta$$

and when integrated gives

$$N = 4nR^2\left[\pi/4 - (4/3)R/\lambda + (\pi/8)(R/\lambda)^2 + \cdots\right]$$

$$= n\pi R^2\left[1 - (16/3\pi)R/\lambda + (1/2)(R/\lambda)^2 + \cdots\right]$$

The total number of photons produced is

$$N_0 = n\pi R^2$$

Therefore, the correction factor becomes

$$N_0/N = \frac{1}{1 - (16/3\pi)R/\lambda + \cdots}$$

which for $R \ll \lambda$ becomes

$$N_0/N \approx 1 + (16/3\pi)R/\lambda + \cdots$$

This correction is not really applicable to the case in which the cylinder axis is parallel to the proton beam, as in Series 4. There are two additional features in this orientation. The boundaries of the region of integration are no longer the circular cross sections of the cylinder, but instead are a series of truncated ellipses. The ellipses are due to the observation at 45° to the cylinder axis; the truncation is caused by the cylinder ends. This would tend to give a smaller correction than that calculated for axis perpendicular to the proton beam. The second feature is that all distances, traveled in the target become longer by a factor $\frac{1}{\cos\theta}$ where $\theta = 45°$ = angle between axis and direction of observation. The integral for this case was set up but not evaluated. Instead the assumption was made that these two new effects would approximately cancel. An argument for this is as follows:

For a long cylinder in this orientation (axis parallel to beam) the ends can be neglected and the correction would just be that of a cylinder with axis perpendicular to the beam but with a $1/\cos\theta$ factor to take care of the ellipticity. Hence, for $t \gg R$, where t = thickness

$$N_0/N = \frac{1}{1-(16/3\pi)(R/\lambda\cos\theta)}$$

$$= \frac{1}{1-2.4\,R/\lambda}$$

Also for a short cylinder the slab correction should be good, so for $t \approx R$

$$N_0/N = \frac{1}{1-\frac{1}{2}\,R/\lambda\cos\theta}$$

$$= \frac{1}{1-0.707\,R/\lambda}$$

Between these two is the perpendicularly oriented cylinder

$$N_0/N = \frac{1}{1-(16/3\pi)\,R/\lambda}$$

$$= \frac{1}{1-1.70\,R/\lambda}$$

Therefore the latter correction was used for Be, B^{10}, B^{nat}, C and Ca where $t \approx 2R$ and the long cylinder case was applied to Li, Na, and K where $3R < t < 7R$.

<u>Targets for Pair Spectrometer Run.</u> The beam diameter in this case was $3\frac{1}{2}$ inches at the targets. The carbon and aluminum targets were placed square with the beam with one inch of target overlapping the beam

in the direction of the pair spectrometer (at 90°) (See Fig. 9).

Again, let

n = number of photons produced per unit strip

λ = mean free path for pair production

δ = distance from edge of target to beam (See Fig. 9).

Using the same sort of integration the correction factor is seen to be

$$N_0/N = \frac{t}{\lambda} \frac{1}{e^{-\delta/\lambda}(1-e^{-t/\lambda})}$$

The factor for lead was different only in the value of δ. δ = 0 for lead.

$$N_0/N = \frac{t}{\lambda} \frac{1}{1-e^{-t/\lambda}}$$

VI. RESULTS

The relative cross sections and relative cross sections per neutron in the nucleus are tabulated in Table VI. The comparisons, in each case, are made to carbon which has an arbitrary value of 6.00 assigned for the cross section (this is to allow comparison with neutron number) and 1.000 for cross section per neutron. The best value for the absolute carbon cross section is given by Crandall and Moyer[27] as 1.8 ± 0.4 mb.

The relative cross sections for elements up to aluminum are plotted in Fig. 10. It can be seen from this that the yield continues to be nearly proportional to the number of neutrons up to aluminum. For the heavier elements this ceases to hold true as shown in Fig. 11. In this case comparison is made to the number of neutrons on the nuclear surface, which is proportional to N $(A^{2/3}/A)$. This seems to be a good fit to the data.

These features of the π^0 yield, namely,

1. Production from neutrons
2. Production from all neutrons at low Z and shielding of the interior neutrons at high Z.

show up quite clearly in a plot of σ/N as a function of A, as seen in Fig. 12. The surface effect, represented by $A^{-1/3}$, now becomes a straight line on the logarithmic plot.

The possibility of seeing other events due to the low energy threshold of the crystal counters is discounted by a comparison with the data obtained using the pair spectrometer at 90°. These results are also

TABLE VI

Elem	A	N	Relative σ	Relative σ	Relative σ/N
H	1	0	0.072 ± 0.060	0.012 ± 0.010	-
H^2	2	1	0.856 ± 0.020	0.143 ± 0.034	0.856 ± 0.020
He	4	2	2.22 ± 0.25	0.369 ± 0.041	1.106 ± 0.123
Li	6.92	3.92	3.42 ± 0.13	0.569 ± 0.021	0.871 ± 0.032
Be	9	5	4.98 ± 0.13	0.830 ± 0.022	0.996 ± 0.027
B^{10}	10	5	4.86 ± 0.13	0.810 ± 0.022	0.973 ± 0.027
B^{11}	11	6	5.93 ± 0.19	0.988 ± 0.032	0.988 ± 0.032
C	12	6	6.000	1.000	1.000
O	16	8	7.51 ± 0.31	1.252 ± 0.051	0.940 ± 0.038
Na	23	12	11.96 ± 0.40	1.991 ± 0.067	0.996 ± 0.047
Al	27	14	12.78 ± 0.70	2.13 ± 0.12	0.914 ± 0.050
Cl	35.5	18.5	13.72 ± 0.62	2.29 ± 0.10	0.782 ± 0.044
K	39	20	16.61 ± 0.60	2.77 ± 0.10	0.830 ± 0.042
Ca	40	20	15.79 ± 0.96	2.63 ± 0.16	0.788 ± 0.046
Cu	63.5	34.5	25.1 ± 1.9	4.18 ± 0.32	0.727 ± 0.057
Pb	207.2	125.2	58.7 ± 3.2	9.79 ± 0.53	0.469 ± 0.026
Pair spectrometer					
C	12	6	6.000	1.000	1.000
Al	27	14	13.32 ± 1.02	2.22 ± 0.17	0.952 ± 0.072
Pb	207.2	125.2	48.2 ± 3.8	8.04 ± 0.62	0.384 ± 0.029

given in Table VI. The aluminum results from the two methods overlap, whereas the lead yield from the pair spectrometer is approximately 20 per cent lower than from crystals. The errors listed are the standard deviations due to random counts and do not include any estimate of system errors. The grossness of the corrections made in the case of the pair spectrometer targets and the number of different measurements and assumptions that went into the calculations for these corrections do not permit one to say the lead yields from the two methods of measurement are significantly different.

The results of the nitrogen - argon comparison are not listed because insufficient cyclotron time was available to get worthwhile statistics.

VII. CONCLUSIONS

The most striking feature of the cross section is the way it differs from the cross section for photon-produced neutral mesons as observed by Panofsky, et al[15]*. For comparison, the cross section per relevant nucleon (proton or neutron for the photo-produced reaction) is plotted against A on a logarithmic plot for the two cases in Fig. 13. For this comparison of shape the two curves have been arbitrarily normalized for lithium.

For the heavy elements both curves fall off as $A^{-1/3}$. The difference lies in the fact that the curve also goes as $A^{-1/3}$ in the light elements for the photo-production case, whereas it becomes constant for the proton induced reaction.

Brueckner, Serber, and Watson[28] have published a paper on this subject in which they point out that a meson yield per nucleon which depends on $A^{-1/3}$, from lithium to lead, sets an upper limit of 2 a_o (where $a_o \approx 1.37 \times 10^{-13}$ cm) on the meson absorption mean free path in nuclear matter. The fact that the yield per nucleon is constant for the light elements in the proton-produced process means that this upper limit no longer applies.

There are three separate effects, each of which could cause a yield dependent on $(N/A)\ A^{2/3}$, as seen among the heavier elements. These effects are:

1. Absorption of the incoming protons.

---

* Silverman in experiments on neutral meson production at the Cornell synchrotron does not see a decline in the yield per nucleon in the low Z elements. The upper limit to the Cornell bremsstrahlung spectrum is 310 Mev.

2. Reabsorption of the meson by the parent nucleon and a near neighbor.

3. Reabsorption by some other nucleon as the meson moves to the nuclear surface.

Protons are absorbed in nuclear matter with a mean free path of approximately 2.5 a_o, where the nuclear radius is given by $R = a_o A^{1/3}$. The effect of this absorption is shown in Fig. 14. The singly shaded section indicates that part of the nucleus in which the proton beam intensity is down by more than a factor of e. In the doubly shaded portion it is down by more than e^2. From the figure, then, one can see that as the nucleus gets bigger, the tendency is to produce mesons in a volume which is of the order λ_p deep and $A^{2/3}$ in area. The number of neutrons per unit volume is just N/A. Hence the dependence $(N/A)\ A^{2/3}$.

The second effect, as was mentioned earlier, depends on the degree to which the meson position can be localized at the time of its creation. As Wilson[31] points out, the reabsorption is of the order of 90 per cent for mesons of greater than 70 Mev. This fraction should be less only for those nucleons on the nuclear surface where there is not the near unit probability of finding a neighboring nucleon within the distance $\hbar/\mu c$. This effect allows only mesons from the surface nucleons to be seen in reasonable numbers.

The third effect is shown in Fig. 15. Here again, the single and double shading represents regions in which the meson probability of escape is less than 1/e and $1/e^2$ respectively. A mean free path of $2a_o$ is shown for the meson reabsorption. Again, as the nucleus becomes larger, the greatest probability is to see mesons created near the surface.

These several effects amount to a screening of some of the neutrons in the heavier nuclei. This screening can be due either to absorption of the incoming protons by other inelastic processes (thus reducing the probability of having collisions at the rear of the nucleus produce mesons) or to reabsorption of the mesons before they can leave the nucleus (thus reducing the probability of escape for mesons produced in the center of the nucleus). Let us assume that the mesons have an infinite mean free path for absorption and investigate the variation of the yield to be expected as a function of A. By assuming an infinite meson mean free path we can see the effect of the first screening.

The proton absorption cross section (including everything but elastic scattering) is given in a formula derived in the appendix and previously given by Fernbach, Serber, and Taylor[29], namely,

$$\sigma_a = \pi a_0^2 A^{2/3} \left\{ 1 - \tfrac{1}{2}(\lambda/R)^2 + e^{-2R/\lambda} \left[\lambda/R + \tfrac{1}{2}(\lambda/R)^2 \right] \right\}$$

where

λ = mean free path for absorption of protons in nuclear matter.

$$= \frac{3A}{4\pi R^3}$$

$R = a_0 A^{1/3}$ = nuclear radius

A curve of relative proton absorption cross sections per nucleon, as calculated above, is shown in Fig. 16 as a comparison with the yield data obtained in this experiment. It cannot be said that there is any substantial difference between the two curves. Even when one considers the errors of approximately 10 per cent associated with the calculated

proton absorption cross section and the observed 3 - 8 per cent of the meson cross section the agreement of the two curves is not appreciably changed.

If one assumes an infinite mean free path for the proton one has the case considered in Brueckner[28] et al. They set

$$\sigma'/N = \eta \sigma f_a$$

where

σ' = cross section of nucleus of mass number A for producing π^0's.

η = effect of nuclear binding

σ = nucleon production cross section for π^0's

f_a = probability of a meson leaving the nucleus in which it is produced

A plot of f_a, for various assumed values of meson mean free path, is given in Fig. 17. If there were no proton screening one could say the curve of Fig. 12 could be described by

$$2a_0 < \lambda < 4a_0 ,$$

approximately.

To get a good estimate of the expected yield would require a complicated integral covering the absorption of both protons and mesons. A first approximation would be to multiply the results of the separately integrated effects. This should be good for λ-meson very large. This approximation is shown for $\lambda = 10\ a_0$ as the broken curve and for $\lambda = 4\ a_0$ as the dotted curve in Fig. 14. A second approximation, assuming the

nucleus to be a slab, gave the same result when mesons coming out in both the forward and backward directions were considered. Using the slab model and considering only those mesons coming out in the backward direction, a lower limit of $\lambda = 4\ a_o$ may be set. These rough comparisons would seem to indicate a meson mean free path $\lambda = 10\ a_o$ or larger.

The question remains, then, as to why the smaller absorption cross section for the (p, π^o) reaction as compared with (γ, π^o)? The best explanation seems to be in the energy dependence of the cross sections. The detection scheme of Panofsky, et al, was such as to define a minimum energy π^o accepted. The detection of γ-γ coincidences in two telescopes separated by angle φ is such as to give the minimum meson velocity as

$$\beta_{min} = \cos \varphi/2$$

For their case of $\varphi = 75^o$ the minimum energy is given as $E_{min} = 85$ Mev. The experiments on charged mesons indicate that for energies of 85 Mev and above the cross sections are geometric[11][12] but decrease below this energy[8][9][10].

The energy spectrum of neutral mesons in the proton initiated events is given by Crandall[30] to have a peak at 40 Mev, with about 25 per cent having energies of 85 Mev or over. Thus the great bulk of the mesons observed in this experiment are of energies at which the absorption cross section should be less than geometric. Where the energy acceptance is so wide and the variation in absorption cross sections so great, as is the case here, the detection of low energy mesons is favored as shown in Fig. 17 (the large mean free paths are associated with small energies). It thus appears reasonable that the difference between the absorption of neutral mesons in the case of proton initiated as compared with photon

initiated reactions may be attributed to the variation in π^0 absorption cross section with energy.

In Fig. 16 it is seen that the meson curve turns down at low A whereas the proton absorption curve continues to rise with decrease in mass number. This would seem to be the only indication of any effect due to internal momenta in the nuclei. For the elements from beryllium on up there seems to be no evidence for such a dependence on nucleon momentum changes, the effect of momentum distributions seems constant. Deuterium and lithium are low - possibly because of lower internal momenta, especially in the case of deuterium.

There was no indication of dependence on binding energy or shell structure. The beryllium yield was not anomalous as would be expected if binding energies were important.

A summary of conclusions, then, is:

1. With the present detection method, and at the π^0 energies available here the reaction (p, π^0) shows little effect of π^0 reabsorption, with the mean free path $\lambda_m \approx 10\ a_0$. This would give $\sigma_m \approx 8$ millibarns as the π^0 absorption cross section per nucleon in nuclear matter.

2. The reaction (γ, π^0) shows strong effects of π^0 reabsorption, with $\lambda_m \approx 2\ a_0$ or $\sigma_m \approx 40$ millibarns for nuclear particles, when relatively high energy π^0's are observed.

3. The difference is presumed to be due to the energy dependence of π^0 absorption, with (γ, π^0) taking place at meson energies over 85 Mev and (p, π^0) over a range of meson energies from zero to approximately 150 Mev, with a peak at 40 Mev.

4. The relatively low yields of deuterium and lithium might be due to their having lower internal momenta than the heavier elements. The production cross section rises rapidly with energy; therefore a slightly lower value of the average nucleon momentum on the part of these two particles as compared to the rest of the periodic series could result in the lower yield.

5. There seems to be no effect of binding energy or shell structure, except as these are related to nucleon momenta.

VIII. PROPOSED EXTENSION OF π^0 YIELD VERSUS "A" EXPERIMENT

The neutral pion characteristics (no charge, $< 10^{-14}$ second mean life) make it impossible to form a π^0 beam to study its absorption in matter. However, as seen from the arguments of Brueckner, et al, the shape of the yield of π^0's as a function of nuclear mass is a crude means of determining just this effect. The problem is most clean-cut in the reaction (γ, π^0) where one need not be concerned with the screening of the interior nucleons from the high energy γ's. The change in efficiency of nucleons for producing mesons is then attributed solely to meson re-absorption.

It is proposed that this be done as an extension of the work of Panofsky, et al by observing the relative cross sections for π^0 production of elements from hydrogen to lead - with special attention to the low mass region - at various meson energies. The energy range can be bracketed by the following means. Detection of γ-γ coincidences permits determination of a low energy boundary through proper choice of the angle between detectors. The upper limit of the synchrotron bremsstrahlung energy spectrum can be varied to give an upper energy limit.

The fixing of energy limits has as a consequence the reduction of the number of events which will be observed. Compensations might be made through use of more efficient counters (a Cerenkov counter system is proposed), faster electronics, and greater solid angles.

IX. ACKNOWLEDGMENTS

The author would like to thank Professor Burton J. Moyer for his support throughout the course of the experiment and for his many suggestions. To Doctor Roger H. Hildebrand and Doctor Norman Knable go much appreciation for their participation in the early part of the experiment, and for the development of the electronics used. Thanks are due to Doctor R. Stephen White for the use of his high pressure gas target and to Mr. Roscoe A. Byrns of the engineering group for the construction and assembling of the gas pumping system. To the cyclotron crew under Mr. James Vale and Mr. Lloyd Houser go my thanks for cooperation on the bombardments. Last of all I wish to thank my wife, Mary Hales, for her continual faith and encouragement and for the extra effort on her part so necessary to the success of this experiment.

This work was supported by the Atomic Energy Commission.

X. APPENDIX

A. Calculation of Proton Absorption Cross Sections

Consider a nucleus of mass A and radius R. The cross section for proton interaction with the nucleons in the nucleus is assumed to be given by the free particle p-p and p-n cross sections. These are both taken as 30 millibarns at the 340 Mev energies involved. The nuclear mean free path for interaction is given as

$$1/\lambda = \frac{A\sigma}{\frac{4}{3}\pi R^3} = 0.0926 \times 10^{39}\,\sigma$$

where

$$\frac{A}{\frac{4}{3}\pi R^3} = \text{numerical density of nucleons in the nucleus}$$

$$R = a_0 A^{1/3}$$

for

σ = 30 millibarns, as above.

λ = 3.60×10^{-13} cm.

The probability of a proton having no interaction while traveling a distance x in a nucleus is

$$e^{-x/\lambda}$$

The probability of being absorbed in the cylindrical annulus of radius ρ is

$$2\pi\rho(1-e^{-2s/\lambda})\,d\rho$$

where

$2s =$ thickness of the nucleus traversed at radius

$s^2 = R^2 - \rho^2$

Then the total absorption cross section is the integral over ρ

$$\sigma_a = 2\pi \int_0^R \left(1 - e^{-\frac{2\sqrt{R^2-\rho^2}}{\lambda}}\right) \rho \, d\rho$$

The first term integrates directly; the second may be integrated by parts to give:

$$\sigma_a = \pi R^2 - \pi\lambda\left[\frac{\lambda}{2} - e^{-\frac{2R}{\lambda}}\left(R + \frac{\lambda}{2}\right)\right]$$

$$= \pi R^2 \left\{1 - \frac{1}{2}\left(\frac{\lambda}{R}\right)^2 + e^{-\frac{2R}{\lambda}}\left[\frac{\lambda}{R} + \frac{1}{2}\left(\frac{\lambda}{R}\right)^2\right]\right\}$$

$$= \pi a_0^2 A^{2/3} \left\{1 - \frac{1}{2}\left(\frac{\lambda}{R}\right)^2 + e^{-\frac{2R}{\lambda}}\left[\frac{\lambda}{R} + \frac{1}{2}\left(\frac{\lambda}{R}\right)^2\right]\right\}$$

XI. REFERENCES

1. E. Gardner and C. M. G. Lattes, Science 107, p 270 (1948)
2. R. Bjorklund, W. Crandall, B. J. Moyer, H. York, Phys Rev 77, 213 (1950)
3. J. Steinberger, W. K. H. Panofsky, and J. Steller, Phys Rev 78, 802 (1950)
4. Y. Tanikawa, Proc Phys Math Soc, Japan, 24, 610 (1940)
5. H. Yukawa, Proc Phys Math Soc, Japan, 17, 48 (1935)
6. W. Y. Chang, Rev Mod Phys, 21, 166 (1949) for references
7. H. L. Anderson, E. Fermi, E. A. Long, R. Martin, and D. E. Nagle, Phys Rev 85, 934 (1952)
8. A. M. Shapiro, Phys Rev 84, 1063 (1951)
9. A. M. Thorndike, E. C. Fowler, W. B. Fowler, and R. P. Shutt, Phys Rev, 85, 929 (1952)
10. P. J. Isaacs, A. M. Sachs, and J. Steinberger, Phys Rev, 85, 803 (1952)
11. R. L. Martin, H. L. Anderson, and G. Yodh, Phys Rev 85, 486 (1952)
12. C. Chedester, P. Isaacs, A. Sachs, and J. Steinberger, Phys Rev, 82, 958 (1951)
13. R. F. Mozley, Phys Rev, 80, 493 (1950)
14. R. M. Littauer and D. Walker, Phys Rev 82, 746 (1951)
15. W. K. H. Panofsky, J. Steinberger, and J. Steller, Phys Rev 86, 180 (1952)
16. D. Hamlin, M. Jakobson, J. Merritt, and A. Shulz, Phys Rev 84, 857 (1951)
17. D. Clark, Phys Rev 81, 313 (1951)
18. N. Knable, thesis, UCRL-1444; R. W. Hales, R. H. Hildbrand, N. Knable, and B. J. Moyer, Phys Rev 85, 373 (1952)
19. W. Heitler, Quantum Theory of Radiation, Oxford Press
20. R. S. White, UCRL-1319

21. Johnston, Bezman, Rubin, Swanson, Corak and Rifkin, MDDC-850

22. S. W. Akin, "The Thermodynamic Properties of Helium", Trans. ASME 72, 751 (1950)

S. W. Akin, "Thermodynamic Properties of Helium at High Pressures and Temperatures", General Electric Co. Report No. 55141. Index No. NP-124.

23. International Critical Tables v. 3, pp. 17, 18

24. Ibid., p. 4.

25. R. H. Hildebrand, N. Knable, and C. E. Leith, UCRL-1517. To be published in Rev. Sci. Inst.

26. A. G. Carlson, J. E. Hooper, and D. T. King, Phil. Mag. 41, 701 (1950)

27. W. E. Crandall and B. J. Moyer, private communication

28. K. A. Brueckner, R. Serber, and K. M. Watson, Phys Rev 84, 258 (1951)

29. S. Fernbach, R. Serber, and T. B. Taylor, Phys Rev 75, 1352 (1949)

30. W. E. Crandall, thesis, UCRL-1637

31. R. R. Wilson, Phys Rev 86, 125 (1952)

32. M. N. Whitehead and C. Richman, Phys Rev 83, 855 (1951)

XII. ILLUSTRATIONS

1. General layout of the experiment.

2. Counter arrangement and schematic of electronics.

3. Arrangement for pair spectrometer run.

4. High pressure target in position in cave, showing from right to left — concrete shielding wall of the cyclotron, snout, lead collimating wall, ionization chamber, target and counter bases, and rack containing bridge coincidence circuits and limiter power supplies.

5. High pressure pumping system - located outside the cave entrance.

6. Counter detail.

7. Schematic drawing for the crystal diode bridge coincidence circuit.

8. Method of integrating to obtain pair production corrections in a slab or cylindrical target.

9. Method of integrating to obtain pair production corrections in pair spectrometer targets.

10. Relative yield of high energy photons (π^{o}'s) from 340 Mev proton bombardment of nuclei up to aluminum.

11. Relative yield of high energy photons (π^{o}'s) from 340 Mev proton bombardment of nuclei up to lead.

12. Relative yield per neutron of high energy photons (π^{o}'s) from 340 Mev proton bombardment.

13. Comparison of the relative yield per relevant nucleon from the reactions (p, π^{o}) and (γ, π^{o}).

14. Schematic representation of the absorption of 340 Mev protons in the nuclei C, Al, Cu, and Pb.

15. Schematic representation of the reabsorption of high energy mesons before leaving the nucleus in which they are formed. A mean free path of 2 a_o is illustrated as being characteristic of this reabsorption for high energies.

16. Probability of producing and seeing a meson, given in terms of proton absorption cross sections per nucleon. A curve is given for the meson mean free path assumed infinite and approximate curves for λ_{meson} values of 10 a_o and 4 a_o.

17. Probability of a meson leaving the nucleus in which it is formed, given for various values of mean free path.

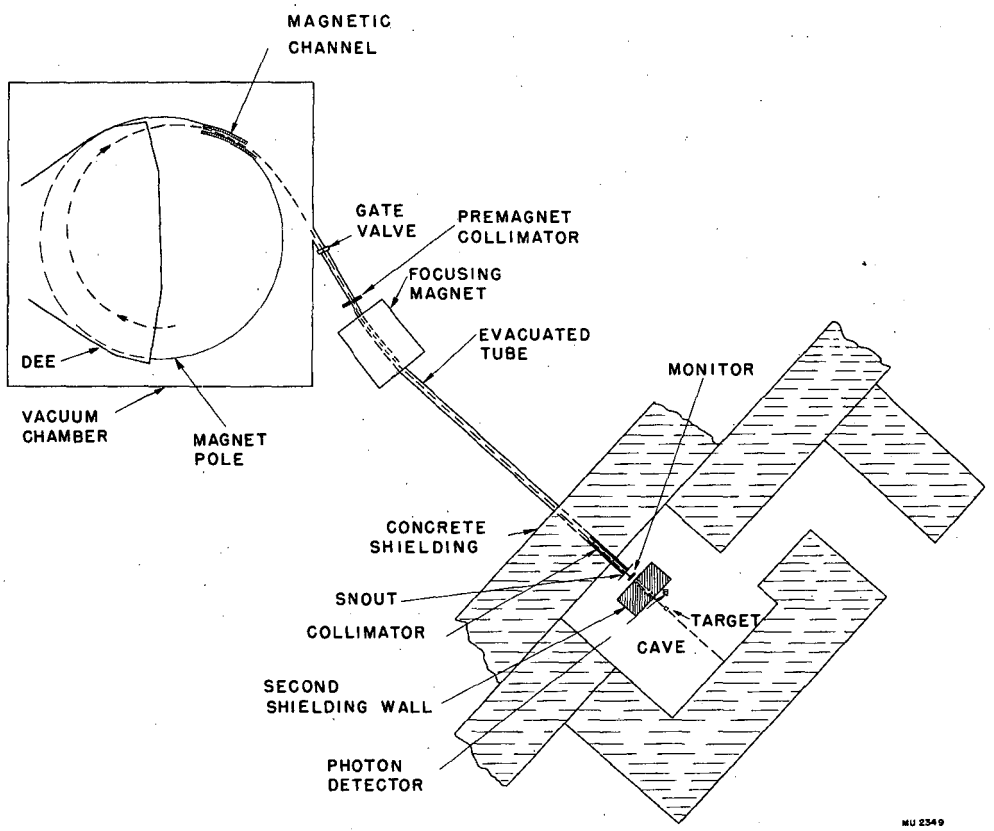

Fig. 1

General layout of the experiment.

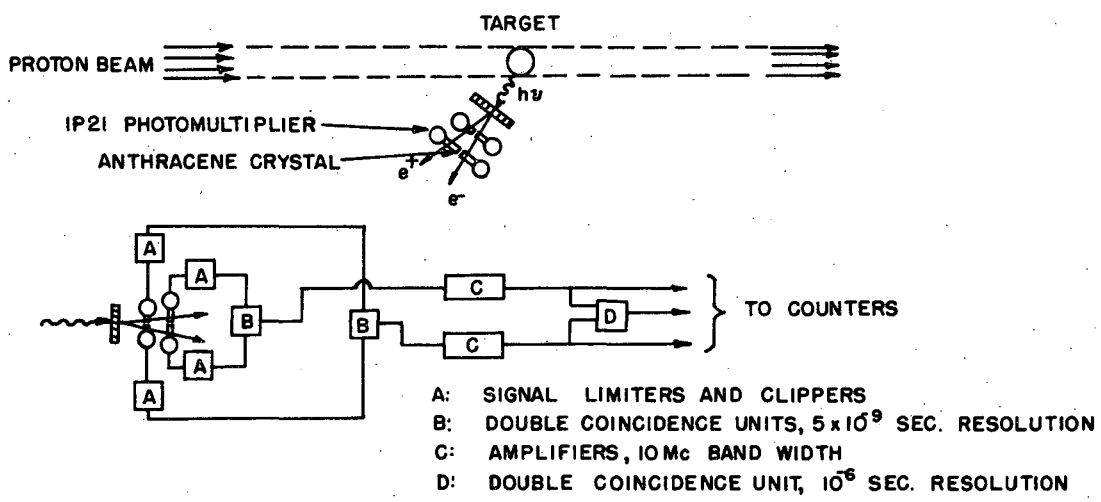

APPARATUS AND CIRCUIT FOR DETECTION OF HIGH-ENERGY PHOTONS

MU3632

Fig. 2

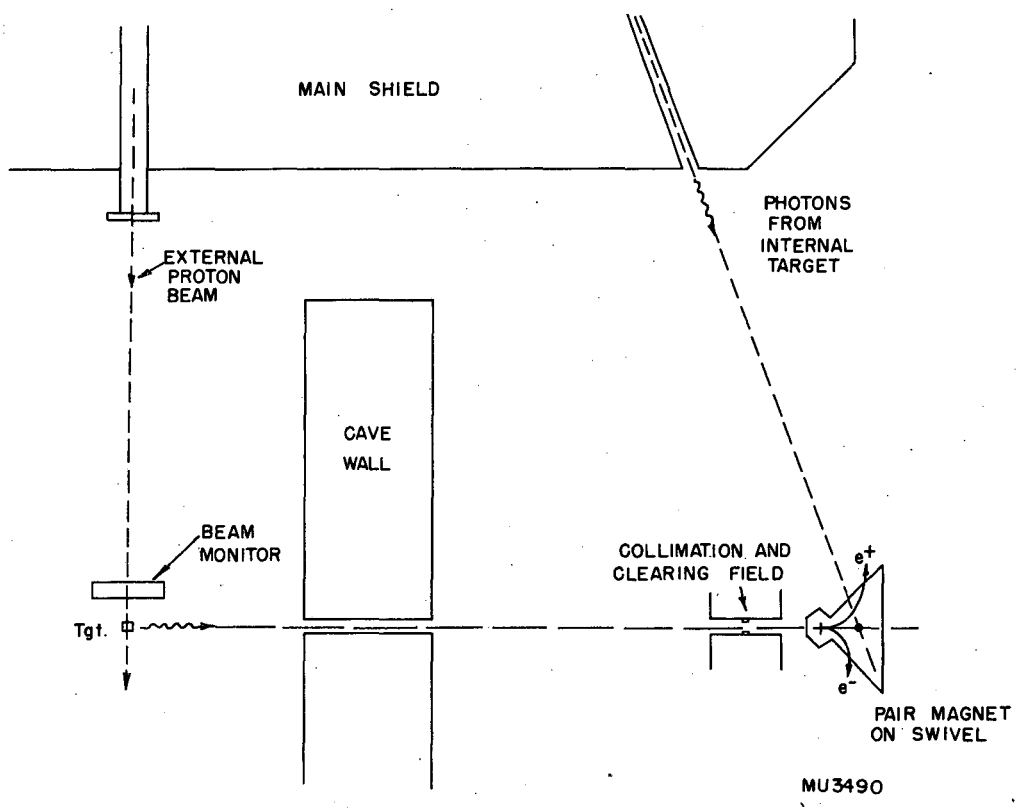

Fig. 3

Arrangement for pair spectrometer run.

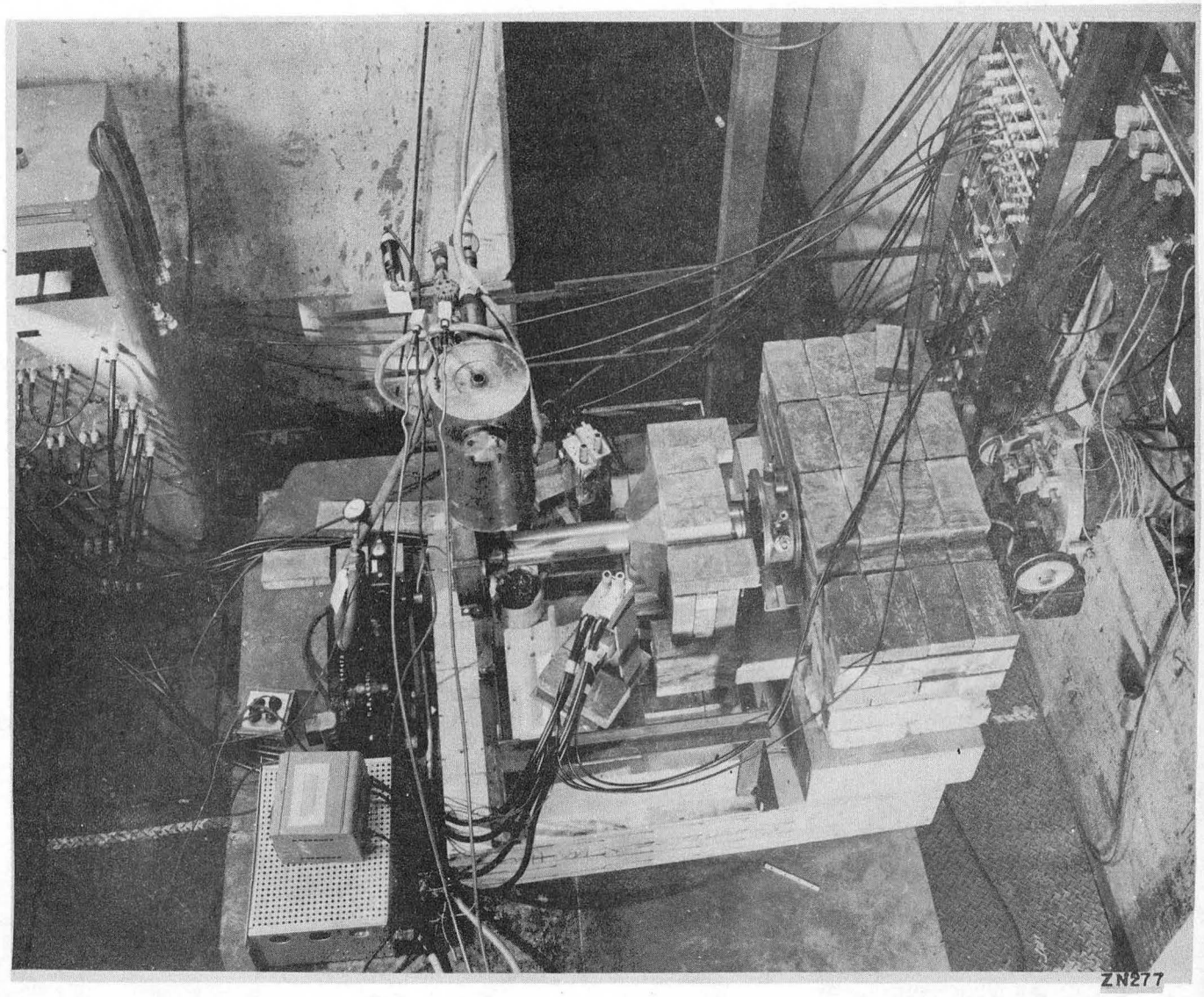

Fig. 4

High pressure gas target.

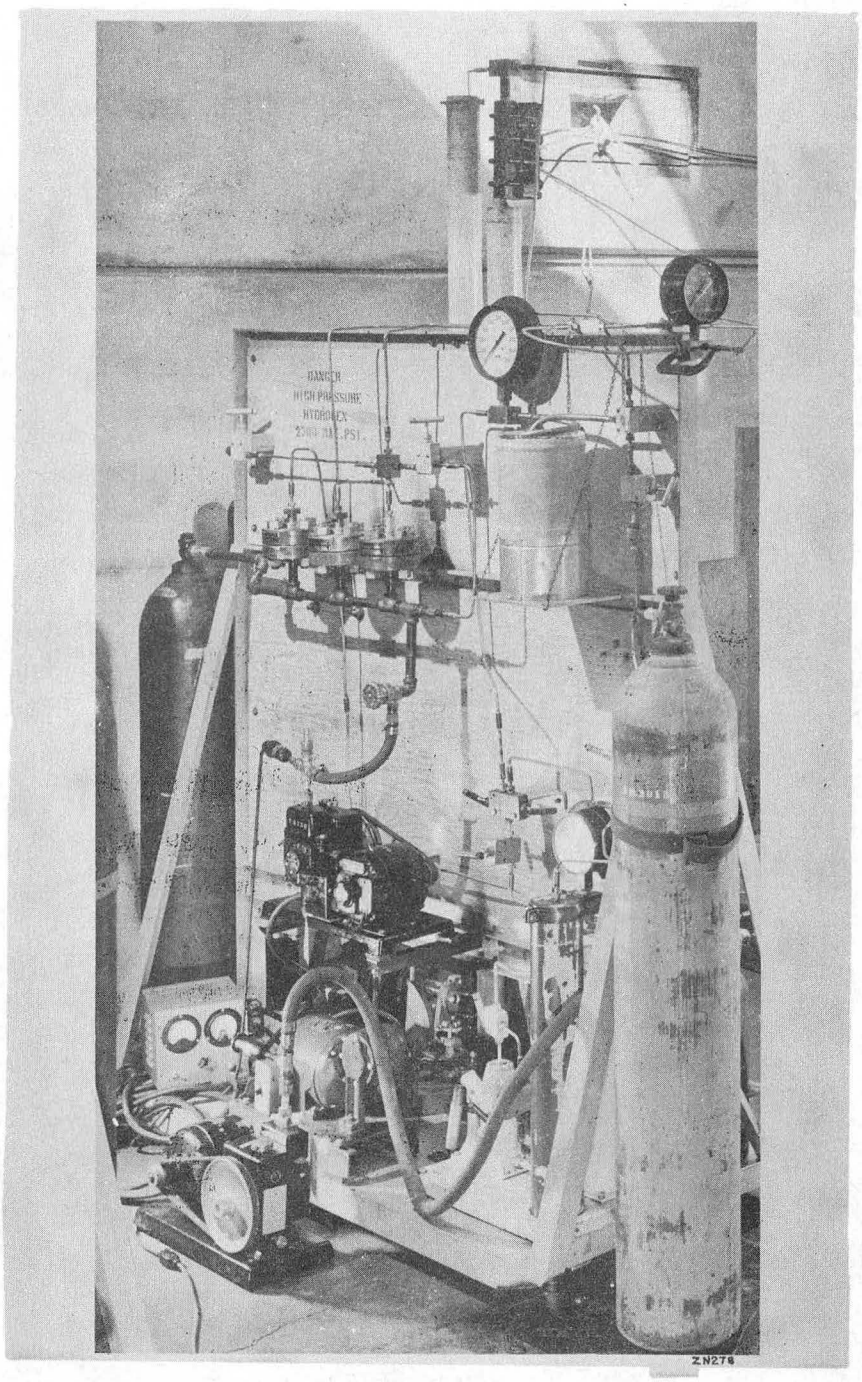

Fig. 5

Pumping system for high pressure target.

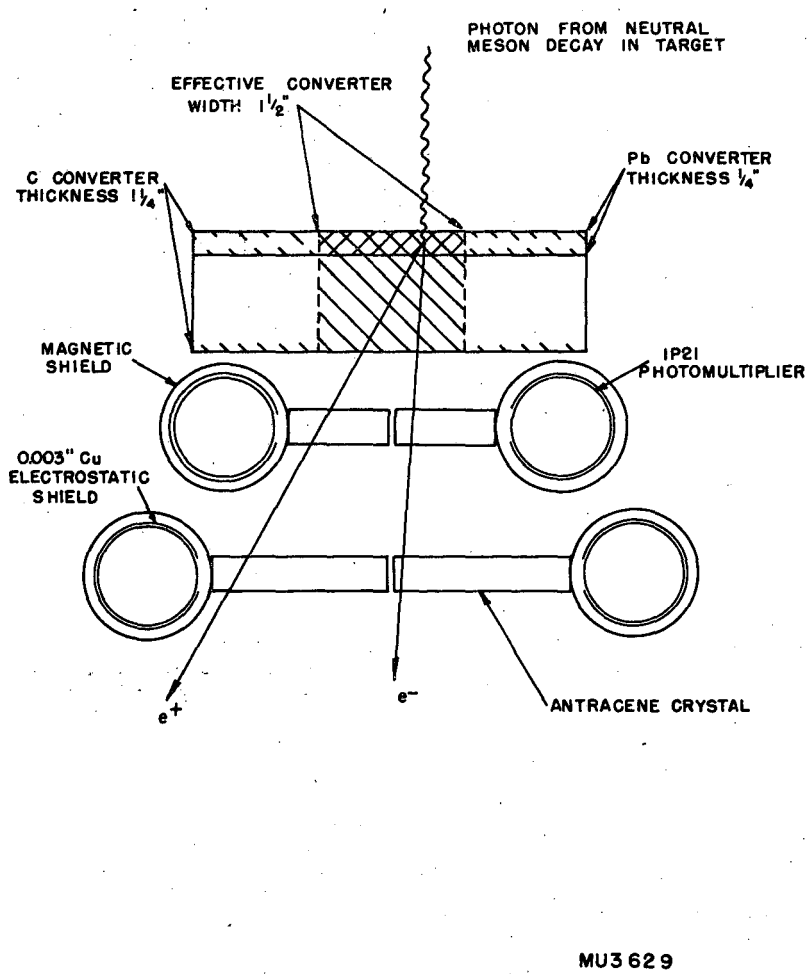

Fig. 6

Photon counter detail.

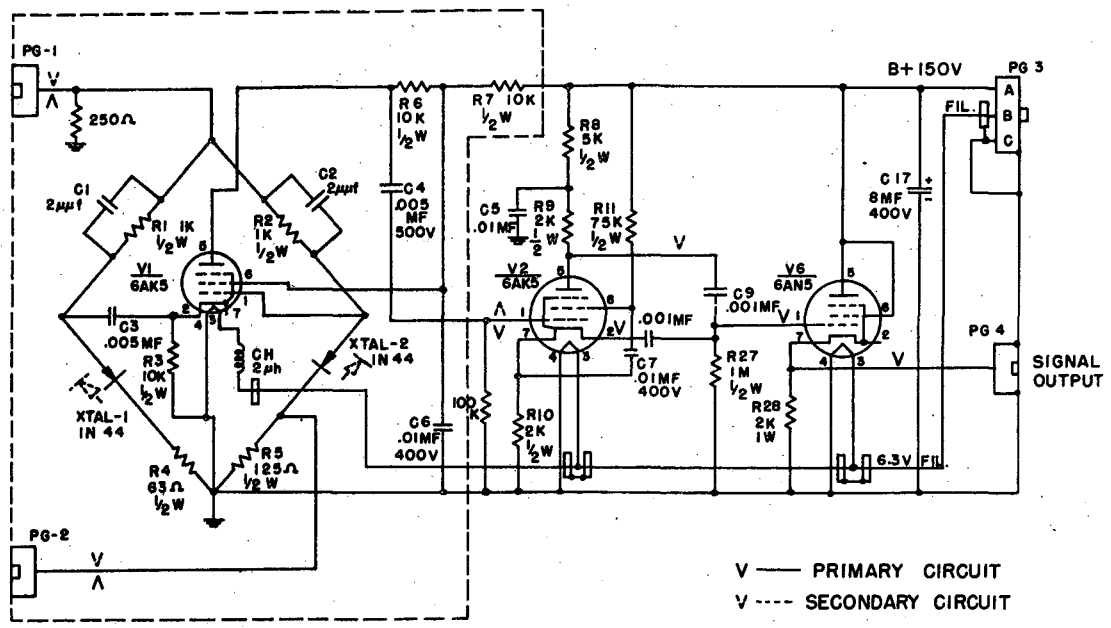

MU3628

Fig. 7

Crystal diode bridge coincidence circuit.

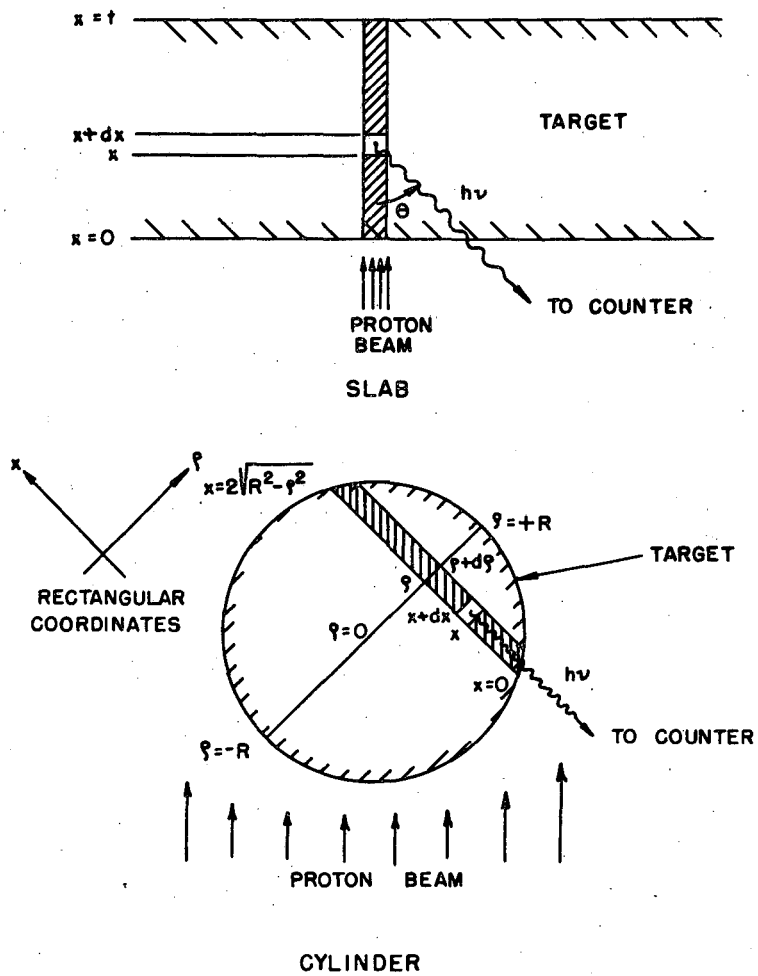
x = t
x+dx
x
x = 0
TARGET
hν
θ
TO COUNTER
PROTON
BEAM
SLAB
x
ρ
x=2√(R²-ρ²)
RECTANGULAR
COORDINATES
ρ=+R
ρ+dρ
TARGET
ρ
ρ=0
x+dx
x
x=0
hν
TO COUNTER
ρ=-R
PROTON BEAM
CYLINDER

MU3630

Fig. 8

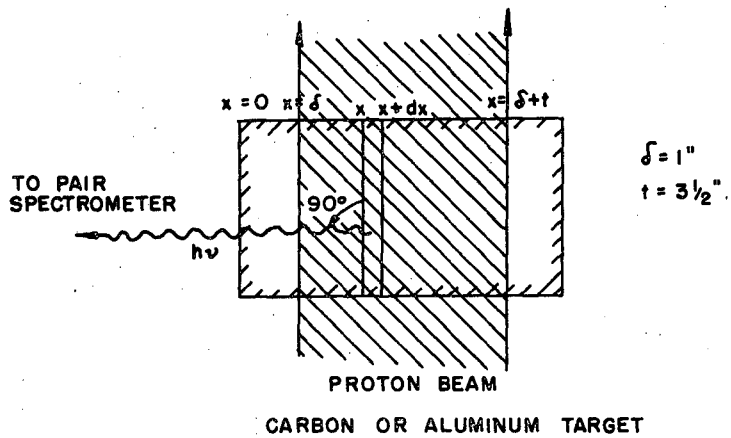
x = 0
x = δ
x
x + dx
x = δ + t
TO PAIR SPECTROMETER
90°
hν
δ = 1"
t = 3½"
PROTON BEAM
CARBON OR ALUMINUM TARGET

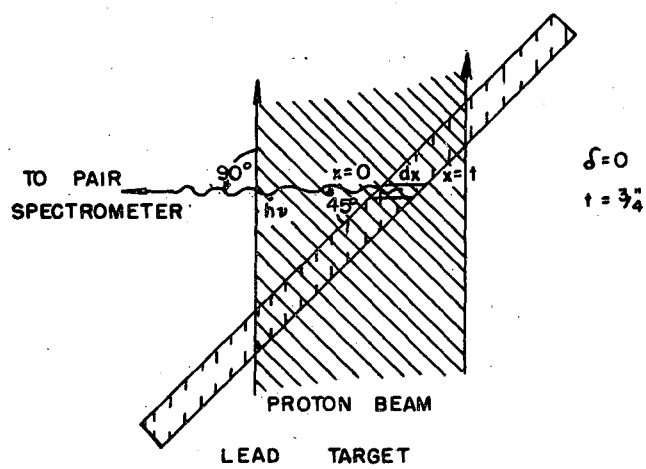
TO PAIR SPECTROMETER
90°
hν
x = 0
dx
x = t
45°
δ = 0
t = ¾"
PROTON BEAM
LEAD TARGET

MU3631

Fig. 9

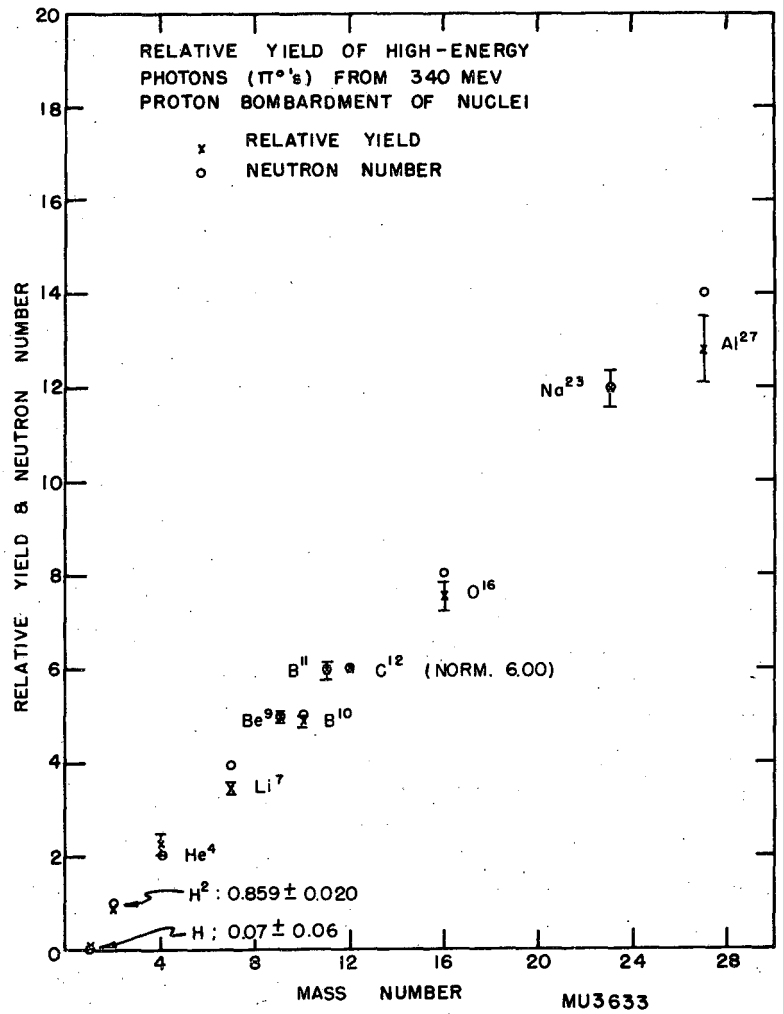
RELATIVE YIELD OF HIGH-ENERGY
PHOTONS (π°'s) FROM 340 MEV
PROTON BOMBARDMENT OF NUCLEI
RELATIVE YIELD
NEUTRON NUMBER
RELATIVE YIELD & NEUTRON NUMBER
MASS NUMBER
Al27
Na23
O16
B11
C12
(NORM. 6.00)
Be9
B10
Li7
He4
H2 : 0.859 ± 0.020
H ; 0.07 ± 0.06
MU3633

Fig. 10

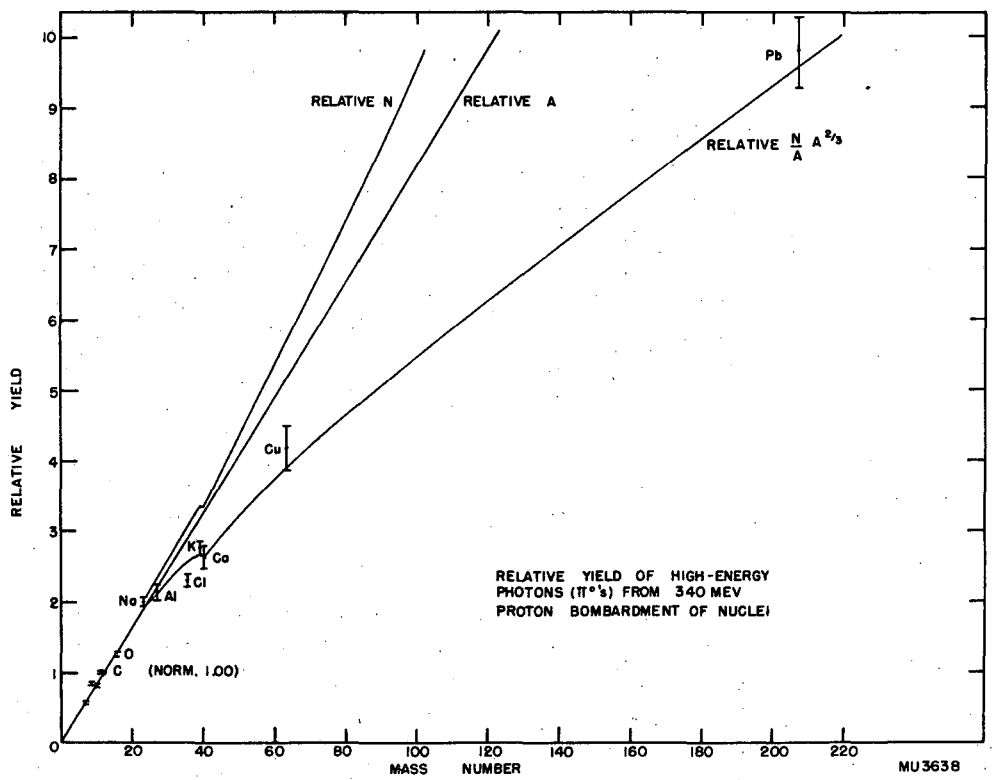
RELATIVE N
RELATIVE A
RELATIVE $\frac{N}{A} A^{2/3}$
Pb
Cu
K
Ca
Cl
Na
Al
O
C
(NORM. 1.00)
RELATIVE YIELD OF HIGH-ENERGY PHOTONS (π^0's) FROM 340 MEV PROTON BOMBARDMENT OF NUCLEI
RELATIVE YIELD
MASS NUMBER
MU3638

Fig. 11

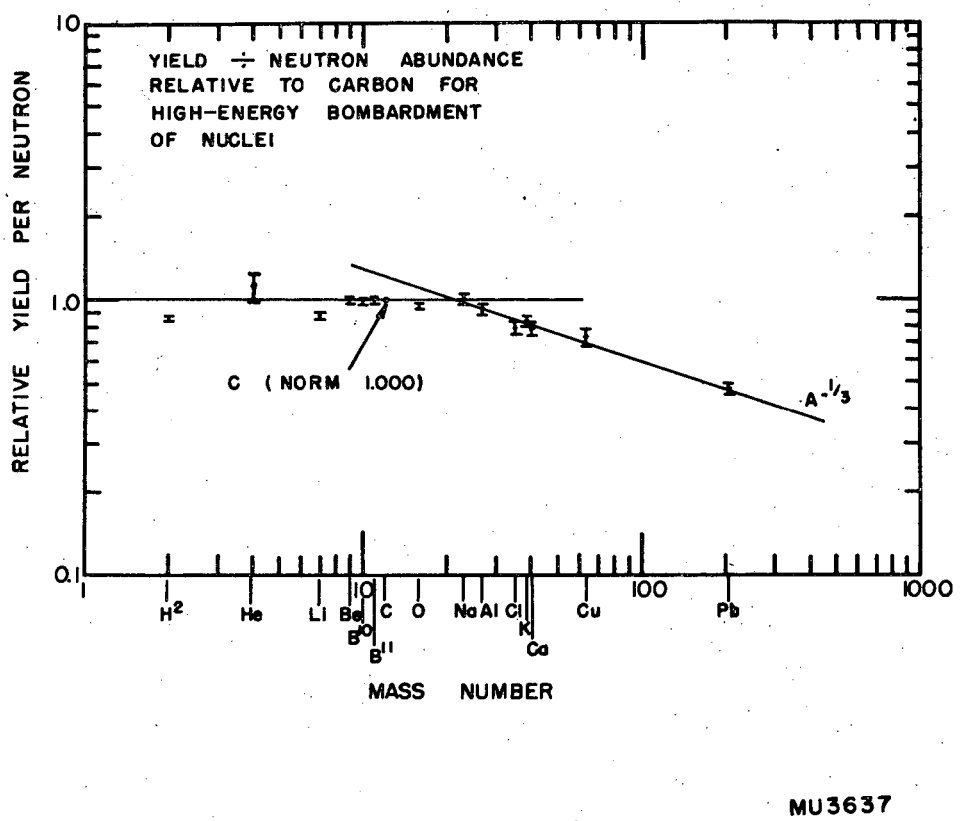

Fig. 12

Relative photon yield per neutron.

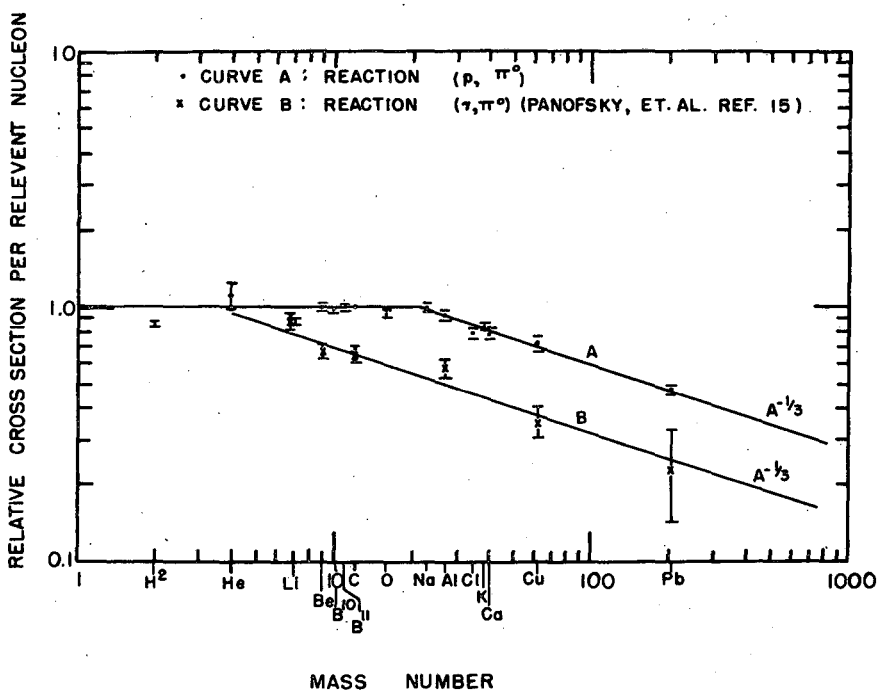

MU3634

Fig. 13

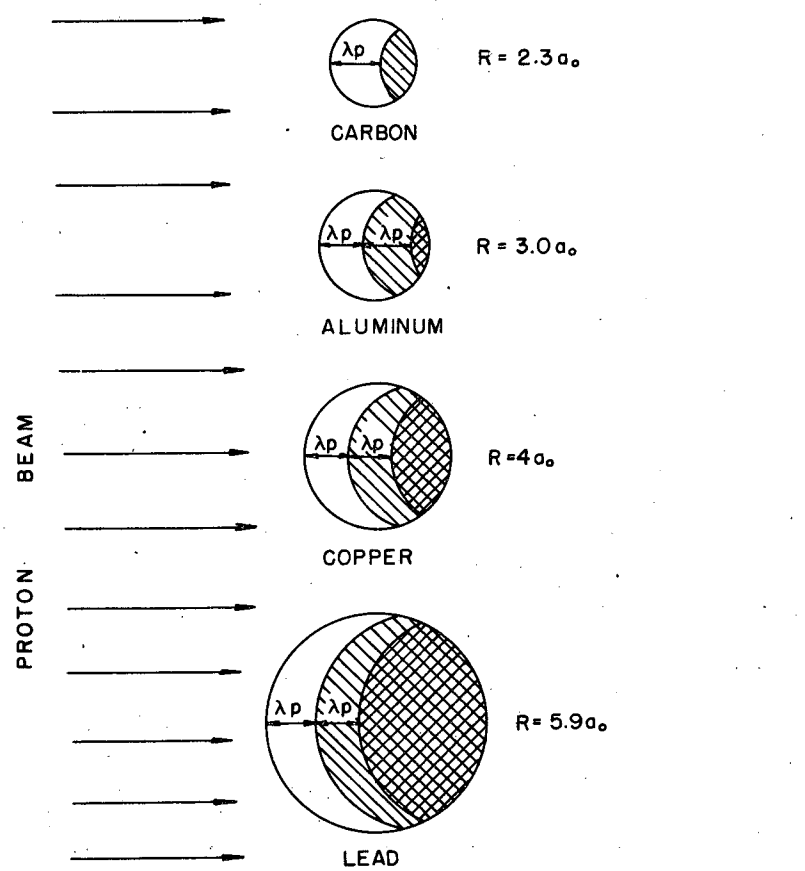

λp = PROTON MEAN FREE PATH FOR INELASTIC COLLISION = 2.5a₀

MU3658

Fig. 14

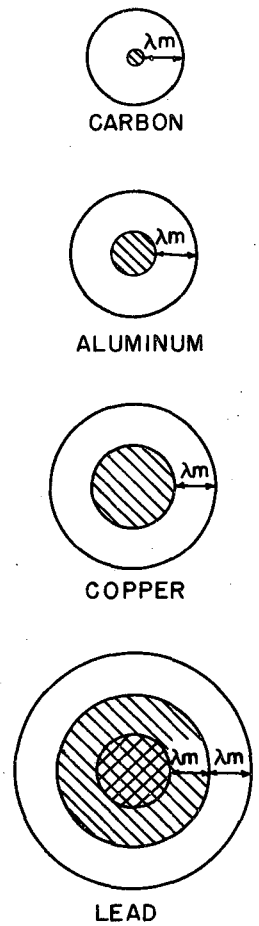

λm = MEAN FREE PATH FOR MESON ABSORPTION

MU3657

Fig. 15

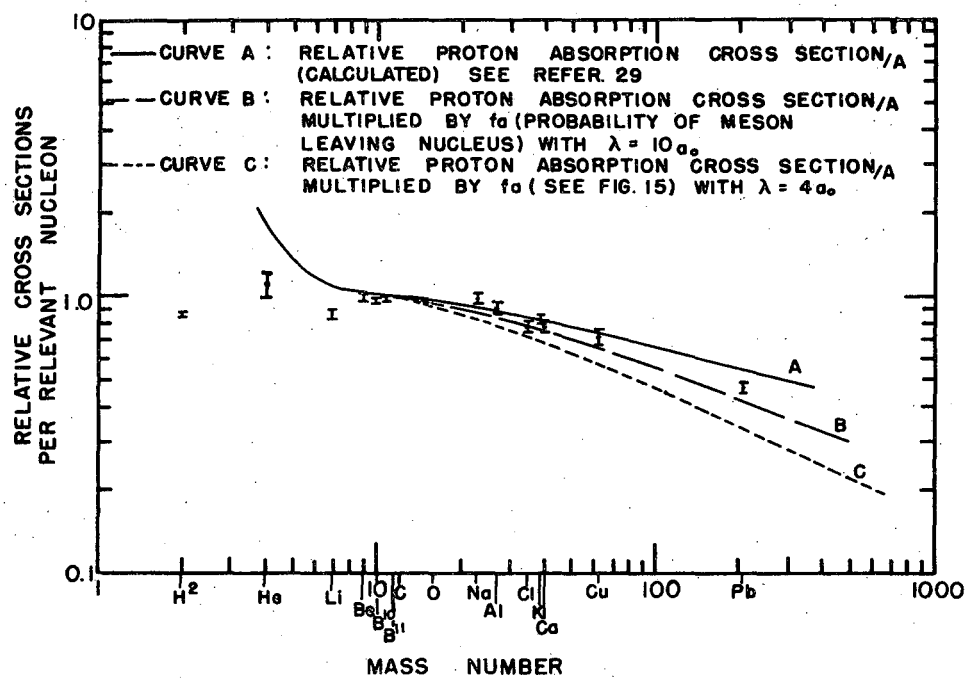

MU3635

Fig. 16

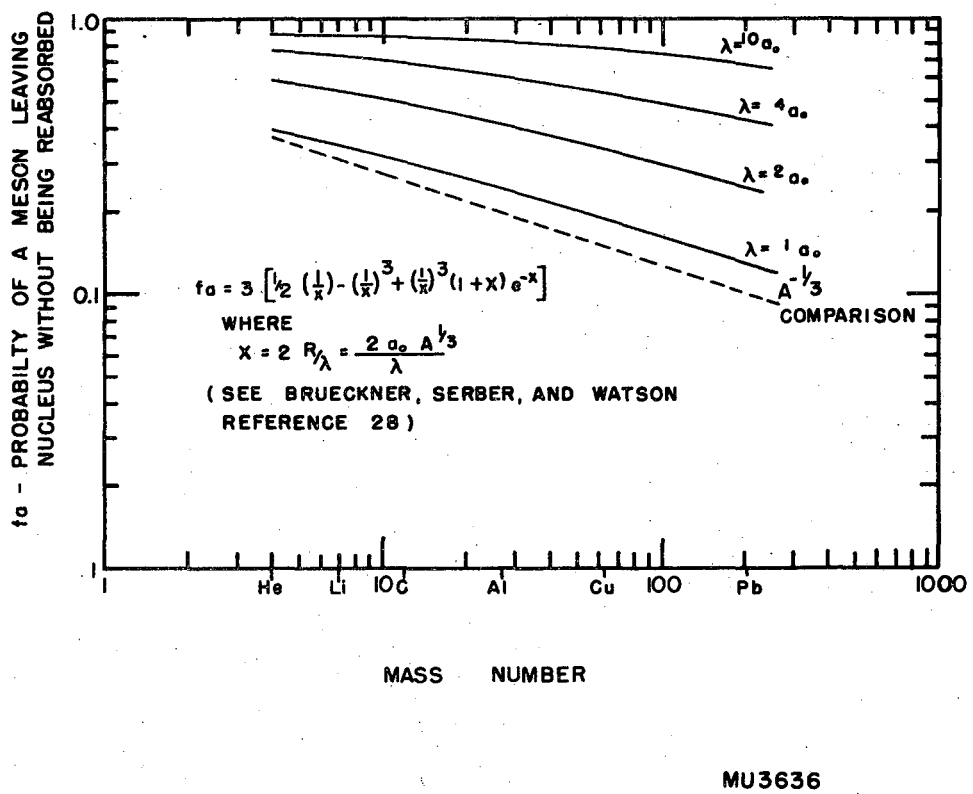

MU3636

Fig. 17